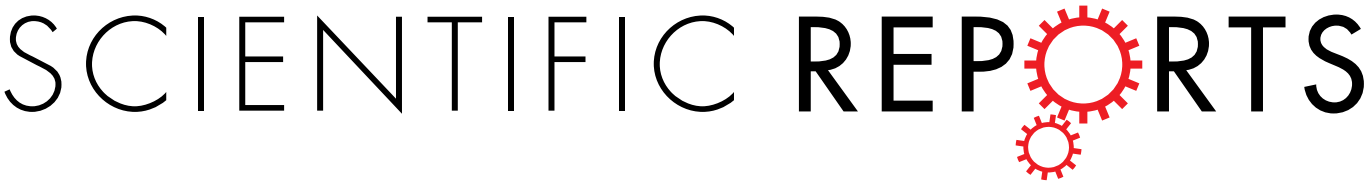

OPEN

Correlation between particle size/ domain structure and magnetic properties of highly crystalline Fe_3O_4 nanoparticles

Received: 28 April 2017
Accepted: 31 July 2017
Published online: 30 August 2017

Qing Li[1], Christina W. Kartikowati[2], Shinji Horie[3], Takashi Ogi[2], Toru Iwaki[2] & Kikuo Okuyama[2]

Highly crystalline single-domain magnetite Fe_3O_4 nanoparticles (NPs) are important, not only for fundamental understanding of magnetic behaviour, but also for their considerable potential applications in biomedicine and industry. Fe_3O_4 NPs with sizes of 10–300 nm were systematically investigated to reveal the fundamental relationship between the crystal domain structure and the magnetic properties. The examined Fe_3O_4 NPs were prepared under well-controlled crystal growth conditions using a large-scale liquid precipitation method. The crystallite size of cube-like NPs estimated from X-ray diffraction pattern increased linearly as the particle size (estimated by transmission electron microscopy) increased from 10 to 64.7 nm, which indicates that the NPs have a single-domain structure. This was further confirmed by the uniform lattice fringes. The critical size of approximately 76 nm was obtained by correlating particle size with both crystallite size and magnetic coercivity; this was reported for the first time in this study. The coercivity of cube-like Fe_3O_4 NPs increased to a maximum of 190 Oe at the critical size, which suggests strong exchange interactions during spin alignment. Compared with cube-like NPs, sphere-like NPs have lower magnetic coercivity and remanence values, which is caused by the different orientations of their polycrystalline structure.

Magnetite (Fe_3O_4) nanoparticles (NPs) have attracted considerable interest as a result of their attractive properties, such as their strong magnetic moment, biocompatibility, chemical stability, and magnetoelectric properties[1]. Numerous reports have described their advances in nanotechnology and their development of a wide range of applications, such as medical application[2], catalysis[3], Li batteries[4], printer toners[5], and wastewater treatment[6]. For the broad application of these NPs, control of the crystal size, shape, and domain structure is important for defining their chemical and physical properties[7]. This was demonstrated in our previous study[8] of photoluminescent NPs, for which the performance was attributable to the domain size rather than the particle size. The particle size, which originates from the magnetic domain structure, has also been recognised as a key factor in the application of magnetic NPs.

The relationship between particle size and the magnetic properties, such as the coercivity (*Hc*), of Fe_3O_4 NPs has been widely reported. The critical size of magnetic NPs, which indicates the transition from a single- to multi-domain structure, was evaluated by the change in *Hc* with respect to the particle size. However, the critical size for Fe_3O_4 NPs has not yet been systematically demonstrated because this value depends on the crystal structure, which can have spherical, cubic, or multiple phases. Therefore, investigation of the critical size on the basis of the crystal structure is necessary.

The particle size required to achieve superparamagnetism in Fe_3O_4 NPs is widely estimated to be below 20 nm[6,9–11], whereas the critical size for forming a multi-domain structure has been theoretically estimated to be 76 nm for cubic[12] and 128 nm for spherical Fe_3O_4 NPs[13]. However, the critical size for cubic Fe_3O_4 NPs has been experimentally determined to be higher than 160 nm[14]. Much smaller critical sizes of 30–46 nm[15–18] have also been reported for cubic Fe_3O_4 NPs. Multi-granule Fe_3O_4 NPs with sizes of 16–512 nm showed a transitional size

[1]Department of Environmental Science and Engineering, Fudan University, Shanghai, 200433, China. [2]Department of Chemical Engineering, Graduate School of Engineering, Hiroshima University, 1-4-1 Kagamiyama, Higashi, Hiroshima, 739-8527, Japan. [3]Technical Strategy Department, Research and Development Division, Toda Kogyo Corporation, Otake, Hiroshima, 739-0652, Japan. Correspondence and requests for materials should be addressed to T.O. (email: ogit@hiroshima-u.ac.jp)

of approximately 120 nm[19]. Although the effects of size and shape on the behaviour of magnetic particles have been known for more than half a century[10], the quantitative effects on $Zn_{0.4}Fe_{2.6}O_4$ NPs remained undiscovered in the size range of 20–140 nm until 2012[20], when the critical size was found to be approximately 60 nm, and the saturation magnetisation (*Ms*) was found to be lower for spherical particles than for cubic ones.

Owing to the experimental difficulty in controlling particle sizes over a wide size range[21], a systematic investigation of the magnetic domain structures of the most commonly used Fe_3O_4 NPs is still lacking, although such an investigation is needed to meet the currently increasing requirements for various applications. The current study therefore investigates the size dependence of the magnetic properties of Fe_3O_4 NPs with sizes of 10–300 nm. The study includes cube- and sphere-like NPs that were produced under well-controlled crystal growth conditions on a large scale. The critical size of highly crystalline cube-like Fe_3O_4 NPs was examined through the correlation between the particle size measured by transmission electron microscopy (TEM) and the crystallite size estimated by X-ray diffraction (XRD). The value was further confirmed by observing the lattice fringes and examining the dependence of *Hc* on the particle size. The high *Hc* value obtained in this study is discussed in detail in terms of the spin interactions in a single-domain structure.

Methods

Two types of highly crystalline Fe_3O_4 NPs, i.e., cube-like and sphere-like ones, were synthesised on a large scale under precise control of the Fe^{2+} concentration, pH, temperature, and aeration rate. The cube-like Fe_3O_4 NPs were prepared by a two-stage oxidation reaction, which is described in patent No. US 5843610A (Toda Kogyo Co., Ltd., Japan)[22]. In contrast, the sphere-like Fe_3O_4 NPs were prepared by a one-stage oxidation reaction, which is described in patent No. US 4992191A (Toda Kogyo Co., Ltd., Japan)[23]. All data generated or analyzed during this study are included in this article and its Supplementary Information files.

The morphologies of the prepared NPs were analysed using field-emission scanning electron microscopy (FE SEM; Hitachi S-5000, Tokyo, Japan) and TEM (JEM-2010, 200 kV, JEOL Ltd., Tokyo, Japan). The crystallite size and chemical composition of the prepared NP samples were examined by XRD (RINT2000, Rigaku Denki Co. Ltd., Tokyo, Japan), using Cu Kα radiation with a scanning range of 2θ 10–80°. Their magnetic performance was assessed using a superconducting quantum interference device (SQUID, Quantum Design, Tokyo, Japan), operated at 300 K. The prepared cube-like NPs with particle sizes (d_p) of 9.6, 19.6, 24.4, 31.9, 45.3, 64.7, 130, 243, and 287 nm were named as C1, C2, C3, C4, C5, C6, C7, C8, and C9, respectively. The sphere-like NPs with d_p of 93.3 and 121 nm were named as S1 and S2, respectively.

Results and Discussion

SEM images of the cube-like Fe_3O_4 NPs are shown in Fig. 1. The d_p of these particles are 9.6, 19.6, 24.4, 31.9, 45.3, 64.7, 130, 243, and 287 nm for C1–C9, respectively, and their size distributions are given in Supplementary Fig. S1. The high-resolution TEM (HRTEM) images of the cube-like Fe_3O_4 NPs in Supplementary Fig. S2 show the lattice fringes of the NPs, and indicate that the NPs have a single crystalline structure up to a d_p of 64.7 nm. In contrast, the C7–C9 NPs, with diameters larger than 100 nm, show a polycrystalline structure. SEM images and size distributions of the sphere-like Fe_3O_4 NPs are shown in Supplementary Fig. S3(a–d). The values of d_p were 93.3 and 121 nm for S1 and S2, respectively. All of the Fe_3O_4 NPs exhibit quasi-narrow size distributions compared with previously reported particles[7,14].

The XRD patterns of cube-like Fe_3O_4 NPs are shown in Fig. 2. The diffraction peaks of 2θ correspond to the [111], [311], [222], [400], [422], [511], and [440] planes, which indicate the pure cubic phase of the Fe_3O_4 NPs. The sharp peaks indicate the highly crystalline nature of the Fe_3O_4 NPs. The XRD patterns of the sphere-like NPs, shown in Supplementary Fig. S3(e), also demonstrate the high crystallinity of these particles. Impurity peaks and transition phases were not observed, which indicates that the particles prepared by the liquid precipitation method were pure, both chemically and in their crystalline phase. The crystallite sizes (d_c) of all the Fe_3O_4 NPs were estimated by the Scherrer formula using the highest intensity XRD peak[24], namely [311], and compared with the d_p obtained from the TEM analysis, as listed in Supplementary Table S1.

The relationship between d_p and d_c is shown in Fig. 3. The straight line indicates a single crystalline particle, whereas the particles corresponding to points that fall below this line are polycrystalline. Notably, the d_c and corresponding d_p have almost the same value for particles with a diameter of 10 to around 80 nm, which indicates a single-domain structure. The particles with diameters of larger than 80 nm have a constant d_c, which indicates a multi-domain structure. The critical size of these cube-like NPs was calculated as 78 ± 9 nm from the relationship between d_p and d_c. The critical size is usually obtained from the change in magnetic properties, such as the relationship of *Hc* and d_p, and this is the first time it has been obtained from the relationship between d_p and d_c for Fe_3O_4 NPs. The same tendency was observed by Lee *et al.*[19] in 2015 for multi-granule Fe_3O_4 NPs, which have a smaller d_c than our NPs. The HRTEM images shown in Supplementary Fig. S2 confirm that NPs with a diameter of up to 64.7 nm have a single crystalline structure, which is shown by the single direction of the lattice fringes. This result is consistent with those obtained for particles produced by a colloidal chemical synthetic route[7,14].

The sphere-like NPs show different crystal properties. For these NPs, the d_c is much smaller than the d_p, and also much smaller than those of the cube-like NPs with a similar d_p, as shown in Supplementary Table S1 and Fig. 3. Supplementary Fig. S4 shows a detailed comparison of the cube-like C7 and sphere-like S2 NPs, which have a similar average d_p. The dark-field TEM image and electron diffraction pattern show that the C7 NP is polycrystalline with a single orientation. However, a polycrystalline structure containing different orientations was observed in the S2 NPs. This was further confirmed from the HRTEM images by the existence of different directions of the lattice fringe in a single S2 NP (Supplementary Fig. S4(g–i)). Sphere-like NPs commonly consist of agglomerates of variously sized cubic NPs[5,14,25]. The different morphological structure arises from the different preparation processes[11], as described in the patent[22,23].

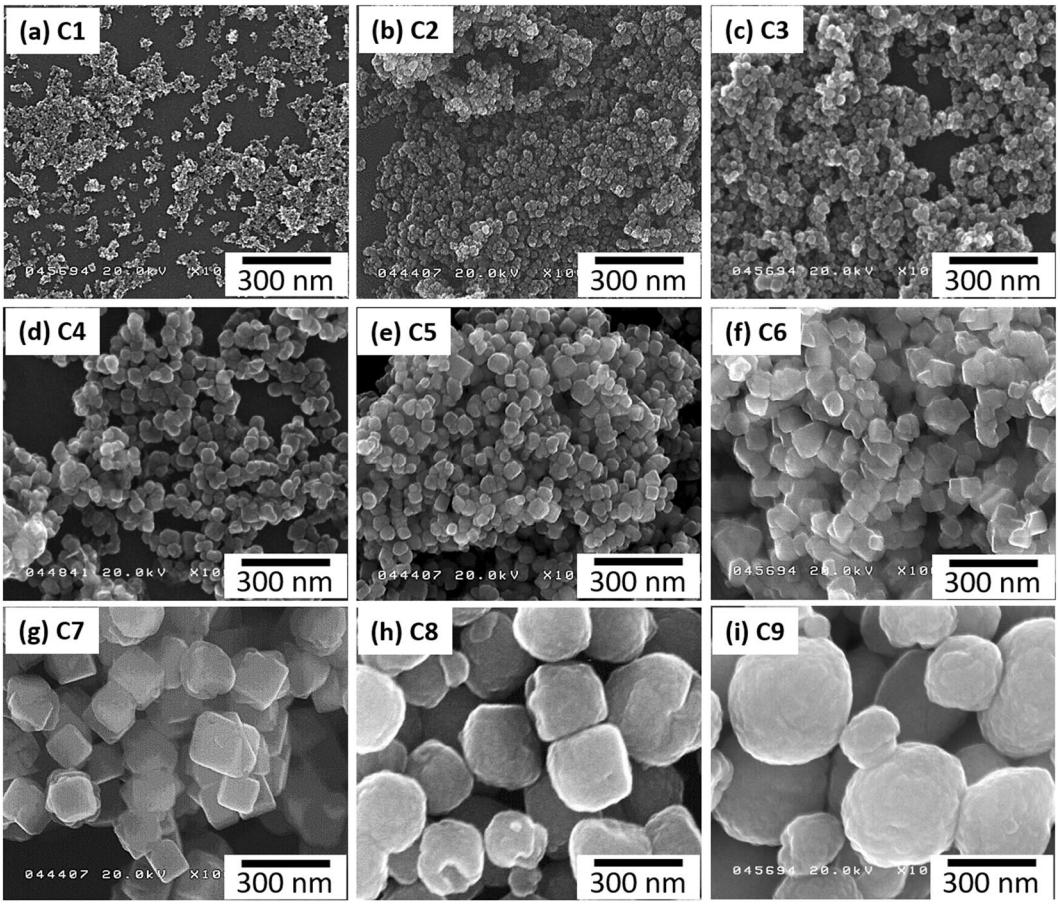

Figure 1. Scanning electron microscopy images of cube-like Fe_3O_4 nanoparticles with various particle sizes. (**a**) 9.6, (**b**) 19.6, (**c**) 24.4, (**d**) 31.9, (**e**) 45.3, (**f**) 64.7, (**g**) 130, (**h**) 243, and (**i**) 287 nm, which are named as C1–C9, respectively.

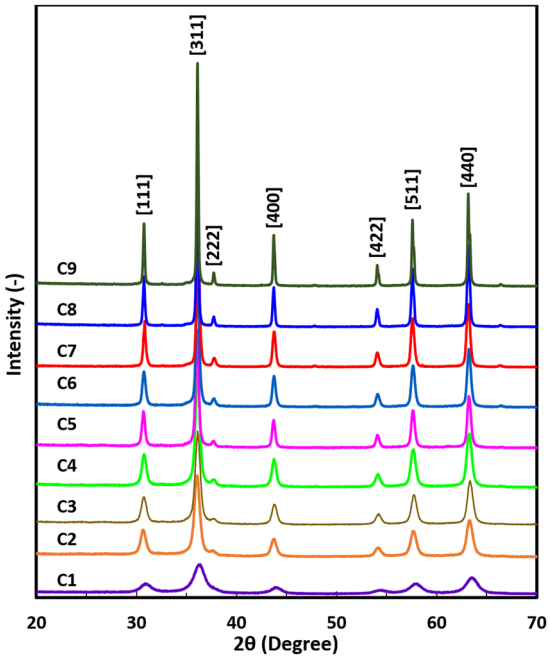

Figure 2. X-ray diffraction patterns of cube-like Fe_3O_4 nanoparticles with various particle sizes.

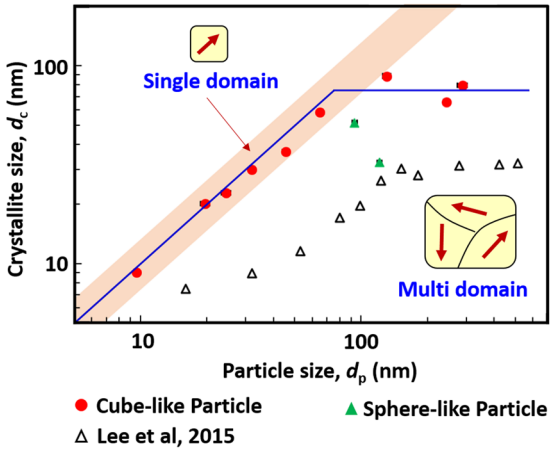

Figure 3. Relationship between average particle size and crystallite size. The solid line shows the trend in the relationship for cube-like Fe_3O_4 nanoparticles. The black open triangles were replotted from Table 1 in ref. 19 for multi-granule Fe_3O_4 nanoparticles.

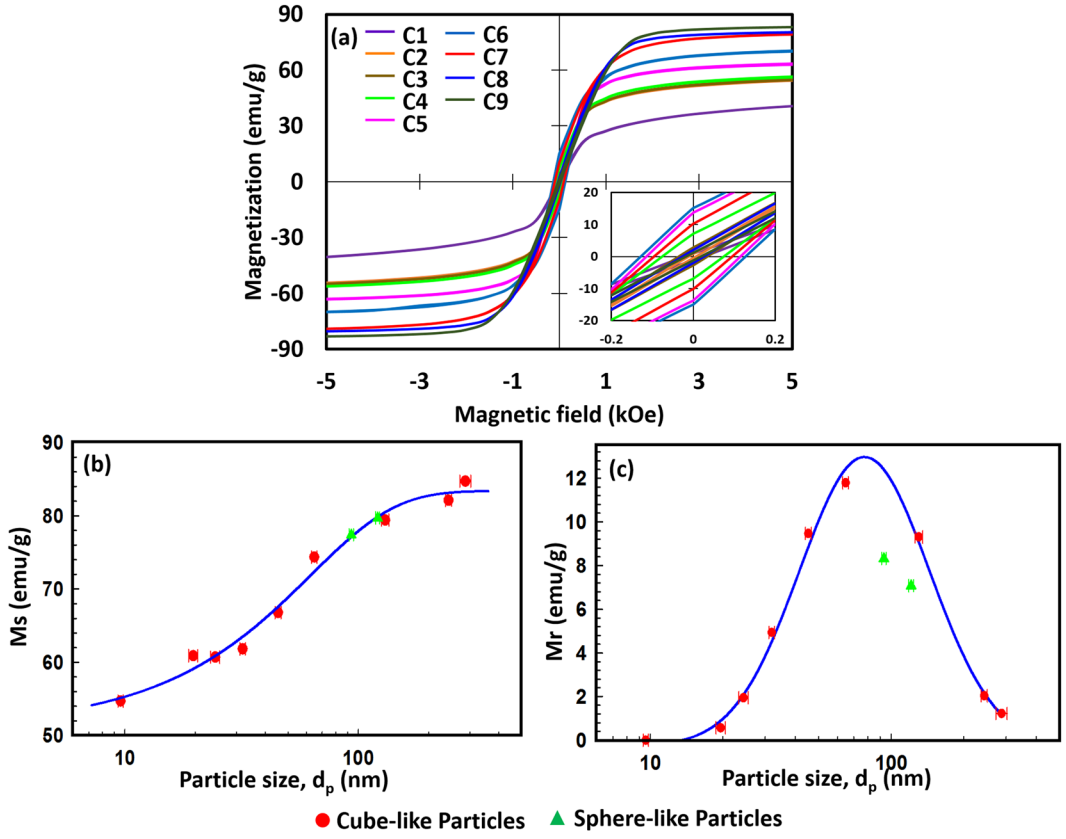

Figure 4. (**a**) Hysteresis loops of cube-like Fe_3O_4 nanoparticles, and particle size dependence of (**b**) saturation magnetization and (**c**) remanent magnetization for all Fe_3O_4 nanoparticles.

The hysteresis loops for these particles, shown in Fig. 4(a), show the ferrimagnetic nature of the Fe_3O_4 NPs. The cube-like Fe_3O_4 NPs possess high *Ms* values, which are affected by the d_p as shown in Fig. 4(b). The *Ms* value, obtained by applying the law of approach to saturation[26], increases with increasing d_p for all samples, including the sphere-like NPs. This trend is consistent with those found in other reports on Fe_3O_4 NPs with diameters lower than 100 nm[5,16,27,28]. The *Ms* value increased from 54.7 emu/g (9.6-nm NPs) to 84.7 emu/g (287-nm NPs), which is close to the theoretically estimated *Ms* for bulk Fe_3O_4 (92 emu/g). The *Hc* and remanent magnetisation (*Mr*), which are also affected by d_p, are shown in Figs 4(c) and 5. These values increase from around 0 for the 9.6-nm NPs, which are known to be superparamagnetic[26,29,30], to a maximum value of around 190 Oe (*Hc*) and 13 emu/g

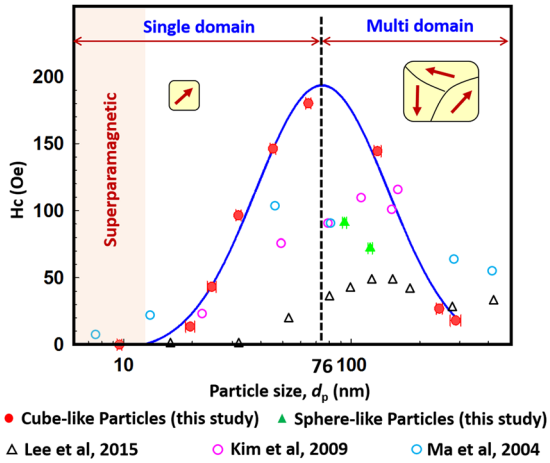

Figure 5. Magnetic performance of Fe_3O_4 nanoparticles measured at 300 K: particle size dependence of the coercivity (*Hc*). The black open triangles, violet open circles, and blue open circles were replotted from refs 14, 15 and 19, respectively.

(*Mr*) at a d_p of around 80 nm, and then decrease continuously with further increases in d_p. The trends in these two parameters are consistent with previous theoretical estimations[10,19,31], and they have similar characteristics to those obtained for $Zn_{0.4}Fe_{2.6}O_4$ NPs[20]. The initial increase in *Hc* with domain size corresponds to the sixth power of the domain size. The high *Hc* value may be caused by the strong spin interactions in highly crystalline Fe_3O_4 NPs during spin alignment, which has previously been observed in soft magnetic NPs[32].

By fitting the measured *Mr* and *Hc* values using a log-normal distribution function, shown by the dark blue solid line, the critical sizes for the maximum *Mr* and *Hc* values were determined to be 77 ± 2 nm and 75 ± 3 nm, respectively. On average, therefore, the critical value for the transition is about 76 ± 4 nm. This value is consistent with the critical size of 76 nm estimated theoretically for the transition from single- to multi-domain behavior[12]. Furthermore, the critical size of about 76 nm is almost the same as the transition size obtained from the relationship of d_c and d_p, as shown in Fig. 3. Single-domain cube-like Fe_3O_4 NPs, such as those with a size of 64.7 nm, can be applied effectively as starting materials for many real products, especially for new rare-earth-free magnets with high magnetic moments, by transformation into α''-$Fe_{16}N_2$ NPs and subsequent dispersion and assembly under a magnetic field[33–38].

The crystalline properties of the NPs affect their magnetic properties, especially *Hc*. The different crystalline properties of the cube- and sphere-like NPs result in their different magnetic performances, as shown in Figs 4(c) and 5. The measured *Mr* and *Hc* values for the sphere-like NPs (S1 and S2) are both lower than the corresponding fitted values for the cube-like NPs. This may be caused by their composite small crystallite size. A comparison of the hysteresis loops of the two NPs with similar d_p (C7 and S2) in Supplementary Fig. S5 shows the difference between the two samples, although their *Ms* values are similar (79.4 and 79.7 emu/g as listed in Supplementary Table S1). The multiple orientations of the polycrystalline in the sphere-like NPs, which lead to the multiple orientations of their easy axes, is considered to be the reason for their lower *Mr* and *Hc* values compared with those of the cube-like NPs. This is consistent with a previous study on the particle-size and shape dependence of Fe_3O_4 NPs[5]. However, further theoretical explanation and experimental investigation are still required.

Conclusions

The magnetic properties, including the *Ms*, *Mr*, and *Hc*, of Fe_3O_4 NPs are highly influenced by the particle size and domain structure. The *Ms* increases with increasing particle size, regardless of the crystal structure and particle shape. After exceeding the superparamagnetic limit, the *Hc* and *Mr* values increase with increasing particle size up to a maximum value of about 190 Oe and 13 emu/g, respectively, at the critical size of 76 nm. Above this critical size, the *Hc* and *Mr* values decrease with further increases in the particle size, and the cube-like Fe_3O_4 NPs change from a single- to multi-domain structure. The multiple orientations of the crystallites within the multi-domain-structured NPs lead to the decrease in the *Hc* value. These findings suggest that considerable attention should be given to the particle size and crystalline properties of Fe_3O_4 NPs, which have potential biomedical and industrial applications. These applications require that magnetic particles are sized appropriately to achieve a good balance between effective surface area and satisfactory magnetic performance.

References

1. Yoo, K., Jeon, B. G. & Chun, S. H. *et al.* Quantitative measurements of size-dependent magnetoelectric coupling in Fe_3O_4 nanoparticles. *Nano Lett.* **16**, 7408–7413 (2016).
2. Ling, D. & Hyeon, T. Chemical design of biocompatible iron oxide nanoparticles for medical applications. *Small* **9**, 1450–1466 (2013).
3. Nie, S., Starodub, E. & Monti, M. *et al.* Insight into magnetite's redox catalysis from observing surface morphology during oxidation. *J. Am. Chem. Soc.* **135**, 10091–10098 (2013).

4. Yamada, T., Morita, K., Kume, K., Yoshikawa, H. & Awaga, K. The solid-state electrochemical reduction process of magnetite in Li batteries: *in situ* magnetic measurements toward electrochemical magnets. *J. Mater. Chem. C* **2**, 5183 (2014).
5. Meisen, U. & Kathrein, H. The influence of particle size, shape and particle size distribution on properties of magnetites for the production of toners. *J. Imaging Sci. Technol.* **44**, 508–513 (2000).
6. Yavuz, C. T., Mayo, J. T. & Yu, W. W. *et al*. Low-field magnetic separation of monodisperse Fe_3O_4 nanocrystals. *Science* **314**, 964–967 (2006).
7. Lee, J., Kwon, S. G., Park, J. G. & Hyeon, T. Size dependence of metal-insulator transition in stoichiometric Fe_3O_4 nanocrystals. *Nano Lett.* **15**, 4337–4342 (2015).
8. Wang, W. N., Widiyastuti, W., Ogi, T., Lenggoro, I. W. & Okuyama, K. Correlations between crystallite: Particle size and photoluminescence properties of submicrometer phosphors. *Chem. Mater.* **19**, 1723–1730 (2007).
9. Jun, Y. W., Huh, Y. M. & Choi, J. S. *et al*. Nanoscale size effect of magnetic nanocrystals and their utilization for cancer diagnosis via magnetic resonance imaging. *J. Am. Chem. Soc.* **127**, 5732–5733 (2005).
10. Huber, D. L. Synthesis, properties, and applications of iron nanoparticles. *Small* **1**, 482–501 (2005).
11. Ozel, F. & Kockar, H. Growth and characterizations of magnetic nanoparticles under hydrothermal conditions: Reaction time and temperature. *J. Magn. Magn. Mater.* **373**, 213–216 (2015).
12. Butler, R. F. & Banerjee, S. K. Theoretical single-domain grain size range in magnetite and titanomagnetite. *J. Geophys. Res.* **80**, 4049–4058 (1975).
13. Leslie-Pelecky, D. L. & Rieke, R. D. Magnetic properties of nanostructured materials. *Chem. Mater.* **8**, 1770–1783 (1996).
14. Kim, D., Lee, N. & Park, M. *et al*. Synthesis of uniform ferrimagnetic magnetite nanocubes. *J. Am. Chem. Soc.* **131**, 454–455 (2009).
15. Ma, M., Wu, Y. & Zhou, J. *et al*. Size dependence of specific power absorption of Fe_3O_4 particles in AC magnetic field. *J. Magn. Magn. Mater.* **268**, 33–39 (2004).
16. Iida, H., Takayanagi, K., Nakanishi, T. & Osaka, T. Synthesis of Fe_3O_4 nanoparticles with various sizes and magnetic properties by controlled hydrolysis. *J. Colloid Interface Sci.* **314**, 274–280 (2007).
17. Santoyo Salazar, J., Perez, L. & de Abril, O. *et al*. Magnetic iron oxide nanoparticles in 10–40 nm range: Composition in terms of magnetite/maghemite ratio and effect on the magnetic properties. *Chem. Mater.* **23**, 1379–1386 (2011).
18. Upadhyay, S., Parekh, K. & Pandey, B. Influence of crystallite size on the magnetic properties of Fe_3O_4 nanoparticles. *J. Alloys Compd.* **678**, 478–485 (2016).
19. Lee, J. S., Myung Cha, J., Young Yoon, H., Lee, J. K. & Kim, Y. K. Magnetic multi-granule nanoclusters: A model system that exhibits universal size effect of magnetic coercivity. *Sci. Rep.* **5**, 12135 (2015).
20. Noh, S. H., Na, W. & Jang, J. T. *et al*. Nanoscale magnetism control via surface and exchange anisotropy for optimized ferrimagnetic hysteresis. *Nano Lett.* **12**, 3716–3721 (2012).
21. Yoo, K., Jeon, B.-G. & Chun, S. H. *et al*. Quantitative Measurements of Size-Dependent Magnetoelectric Coupling in Fe3O4 Nanoparticles. *Nano Lett* **16**, 7408–7413 (2016).
22. Uchida, N., Fujioka, K., Aoki, K., Misawa, H. & Kozawa, M. Magnetic particles for magnetic toner and process for producing the same. Japan patent (1998).
23. Mori, K., Kawabata, M., Kunishige, M., Horiishi, N. & Toda, K. Sphere-like magnetite particles and a process for producing the same. Japan patent (1991).
24. Sun, S. & Zheng, H. Size-controlled synthesis of magnetite nanoparticles. *J. Am. Chem. Soc.* **124**, 8204–8205 (2002).
25. Baumgartner, J., Dey, A. & Bomans, P. H. *et al*. Nucleation and growth of magnetite from solution. *Nat. Mater.* **12**, 310–314 (2013).
26. Klokkenburg, M., Vonk, C. & Claesson, E. M. *et al*. Direct imaging of zero-field dipolar structures in colloidal dispersions of synthetic magnetite. *J. Am. Chem. Soc.* **126**, 16706–16707 (2004).
27. Goya, G. F., Berquó, T. S., Fonseca, F. C. & Morales, M. P. Static and dynamic magnetic properties of spherical magnetite nanoparticles. *J. Appl. Phys.* **94**, 3520–3528 (2003).
28. Caruntu, D., Caruntu, G. & O'Connor, C. J. Magnetic properties of variable-sized Fe_3O_4 nanoparticles synthesized from non-aqueous homogeneous solutions of polyols. *J. Phys. D: Appl. Phys.* **40**, 5801 (2007).
29. Kovalenko, M. V., Bodnarchuk, M. I. & Lechner, R. T. *et al*. Fatty acid salts as stabilizers in size- and shape-controlled nanocrystal synthesis: The case of inverse spinel iron oxide. *J. Am. Chem. Soc.* **129**, 6352–6353 (2007).
30. Kandasamy, G. & Maity, D. Recent advances in superparamagnetic iron oxide nanoparticles (SPIONs) for *in vitro* and *in vivo* cancer nanotheranostics. *Int. J. Pharm.* **496**, 191–218 (2015).
31. Néel, L. Propriétés d'un ferromagnétique cubique en grains fins. *CR Acad. Sci. Paris* **224**, 1488–1490 (1947).
32. Herzer, G. Nanocrystalline soft magnetic materials. *J. Magn. Magn. Mater.* **157/158**, 133–136 (1996).
33. Ogi, T., Li, Q. & Horie, S. *et al*. High-purity core-shell α''-$Fe_{16}N_2/Al_2O_3$ nanoparticles synthesized from α-hematite for rare-earth-free magnet applications. *Adv. Powder Technol.* **27**, 2520–2525 (2016).
34. Ogi, T., Zulhijah, R., Iwaki, T. & Okuyama, K. Recent progress in nanoparticle dispersion using bead mill. *KONA Powder and Particle Journal* **34**, 3–23 (2017).
35. Kartikowati, C. W., Suhendi, A. & Zulhijah, R. *et al*. Effect of magnetic field strength on the alignment of α''-$Fe_{16}N_2$ nanoparticle films. *Nanoscale* **8**, 2648–2655 (2016).
36. Ogi, T., Nandiyanto, A. B. D. & Okuyama, K. Nanostructuring strategies in functional fine-particle synthesis towards resource and energy saving applications. *Adv. Powder Technol.* **25**, 3–17 (2014).
37. Kartikowati, C. W., Suhendi, A. & Zulhijah, R. *et al*. Preparation and evaluation of magnetic nanocomposite fibers containing α''-$Fe_{16}N_2$ and α-Fe nanoparticles in polyvinylpyrrolidone via magneto-electrospinning. *Nanotechnology* **27**, 025601 (2016).
38. Suhendi, A., Kartikowati, C. W. & Zulhijah, R. *et al*. Preparation and characterization of magnetic films of well-dispersed single domain of core–shell α''-$Fe_{16}N_2/Al_2O_3$ nanoparticles. *Adv. Powder Technol.* **26**, 1618–1623 (2015).

Acknowledgements

This work was supported by JSPS KAKENHI Grant Number 26709061 and 16K13642. This work was partly supported by the Center for Functional Nano Oxide at Hiroshima University. The authors also gratefully acknowledge the Ministry of Education, Culture, Sports, Science, and Technology (MEXT) of Japan for providing scholarships (C. W. K.). The authors further thank Prof. Takahiro Onimaru, Prof. Toshiro Takabatake, and Prof. Hiroshi Fukuoka from Hiroshima University. We also thank Dr. Makoto Maeda of NBARD, Hiroshima University, for his assistance with the TEM analysis.

Author Contributions

Contributions of each Author is as follows: Qing Li: Writer of the manuscript and conducted the analyses. Christina W. Kartikowati: Writer of the manuscript and conducted the analyses. Shinji Horie: Synthesis of nanoparticles. Takashi Ogi: Supervision on manuscript writing and analyses. Toru Iwaki: Supervision on manuscript writing and analyses. Kikuo Okuyama: Supervision on manuscript writing and analyses.

Additional Information

Supplementary information accompanies this paper at doi:10.1038/s41598-017-09897-5

Competing Interests: The authors declare that they have no competing interests.

Publisher's note: Springer Nature remains neutral with regard to jurisdictional claims in published maps and institutional affiliations.